THE JOURNAL OF PHYSICAL CHEMISTRY B

Article

pubs.acs.org/JPCB

Improving the CHARMM Force Field for Polyunsaturated Fatty Acid Chains

Jeffery B. Klauda,*[,†] Viviana Monje,[†] Taehoon Kim,[‡] and Wonpil Im[‡]

[†]Department of Chemical and Biomolecular Engineering, University of Maryland, College Park, Maryland 20742, United States

[‡]Department of Molecular Biosciences and Center for Bioinformatics, The University of Kansas, 2030 Becker Drive, Lawrence Kansas 66047, United States

Supporting Information

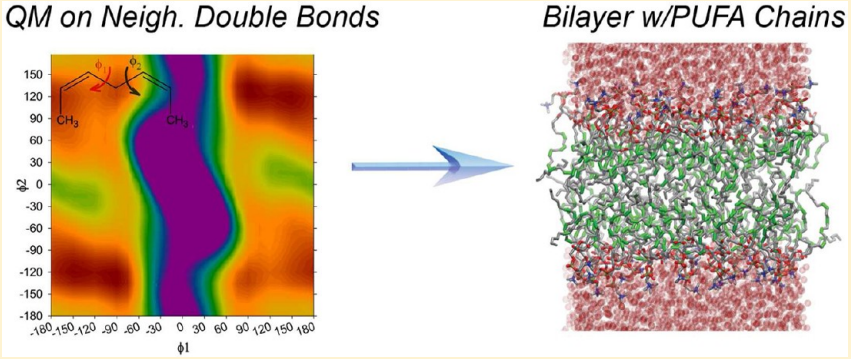

ABSTRACT: CHARMM36 (C36) is the most up-to-date pairwise additive all-atom lipid force field and is able to accurately represent bilayer properties of saturated and monounsaturated lipid molecules in the natural constant particle, pressure, and temperature (NPT) ensemble. However, molecular dynamics (MD) simulations on 1-stearoyl-2-docosahexaenoyl-*sn*-glycerco-3-phosphocholine (SDPC) bilayers of the polyunsaturated fatty acid (PUFA) chains result in inaccuracies of the surface area per lipid (SA), deuterium order parameters (S_{CD}), and X-ray form factors. Therefore, in this study, high-level quantum mechanical calculations are used to improve the dihedral potential of neighboring double bonds, and the corresponding force field is referred to as C36p. The SA for SDPC at 303 K increases from 63.2 ± 0.2 (C36) to 70.8 ± 0.2 (C36p) Å^2 and agrees favorably with X-ray diffraction results at 297 K. The resulting S_{CD} are in excellent agreement with experimental values of both the *sn*-1 and *sn*-2 chains. Calculated NMR ^{13}C relaxation times and X-ray form factors from MD simulations of SDPC bilayers also agree with experiments. MD simulations of 1,2-diarachidonyl-phosphatidylcholine (DAPC) bilayers are used to further validate our force field parameters on a lipid with both chains containing PUFAs. As expected, the thickness of DAPC bilayers is reduced, and the SA is increased compared to the SDPC bilayers. This update in the PUFA force field should allow for accurate MD simulations of PUFA-containing bilayers in the NPT ensemble.

1. INTRODUCTION

Lipids are one of the four major building blocks in biology, which play an integral role in cell stability, preventing unwanted molecules from transporting across the membrane[1,2] and can act as signaling molecules for proteins.[3,4] These amphiphilic molecules can be divided into a headgroup and hydrophobic tails. The headgroup can be ionic or zwitterionic, and the lipid tails can be quite diverse and contain fully saturated chains, mono- or polyunsaturated chains, branched chains, or chains containing cyclic moieties in place of chain unsaturations. In particular, lipid molecules with polyunsaturated fatty acid (PUFA) are important for proper brain function and development, and PUFAs typically exist in three forms (ω-3, ω-6, and ω-9 fatty acids). Liposomes with PUFA-containing lipids have been shown to be antiviral against hepatitis B and C and HIV by possibly reducing cholesterol levels of infected cells,[5] because cholesterol dislikes PUFA-containing lipids. NMR experiments on cholesterol in PUFA-only lipid bilayers have shown that cholesterol orients itself parallel to the membrane surface at the center of the lipid bilayer.[6,7] Such sterol orientational preference is linked to the disordered chains of PUFA-containing lipids and likely results in sterol segregation into liquid ordered domains devoid of PUFA-containing lipids.

Molecular simulations on lipids with PUFAs have been successful in describing lipid biophysical properties,[8−11] cholesterol placement,[11−13] and studies with various integral membrane proteins.[14−17] The CHARMM lipid force field (FF), one of the commonly used all-atom FFs, has parameters for PUFA-containing lipids and was developed based on the

Received: April 26, 2012
Revised: May 30, 2012
Published: June 14, 2012

CHARMM27 (C27) lipid parameter set. In addition, united-atom and particularly course-grained FFs[12,13] have been successful in representing these lipids. Previously, all-atom lipid FFs, such as C27 and C27r, required an imposed surface tension or surface area per lipid for most lipid bilayers to prevent condensation in the constant number of particles, pressure, and temperature (NPT) ensemble.[18,19] This deficiency was resolved with the recent CHARMM36 (C36) lipid FF that accurately represented the structure and dynamics of various lipids with fully saturated and monounsaturated lipid chains.[20]

Although the dihedral potential for alkanes or fully saturated chains was transferrable from C27r to C36, improvements in the monounsaturated dihedral were required to match experimental deuterium order parameters.[20] However, C27-based parameters or C36-based parameters with the NPT ensemble resulted in inaccurate descriptions of surface area per lipid and deuterium order parameters, demonstrating the need to improve this portion of the FF. This paper describes the modification to the PUFA CHARMM FF that is applicable to the C36 parameter set with the NPT ensemble. High-level ab initio quantum mechanical (QM) methods were used to guide the fitting of two dihedral potentials for the PUFA chains. The accuracy of this FF, referred to as C36p, is compared to NMR and X-ray diffraction experiments of bilayers with 1-stearoyl-2-docosahexaenoyl-sn-glycerco-3-phosphocholine (SDPC) and 1,2-diarachidonyl-phosphatidylcholine (DAPC) (see Figure 1A,B for the chemical structure of these lipids).

2. METHODS

Since QM calculations with accurate inclusion of electron correlation and large basis sets are demanding, 2,5-heptadiene

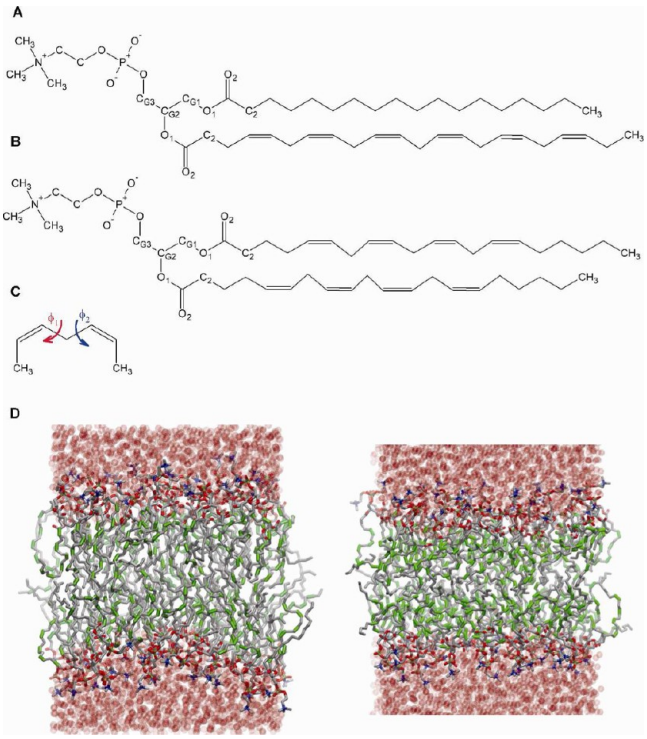

Figure 1. Chemical structures of (A) SDPC, (B) DAPC, and (C) a model compound for the development of the polyunsaturated force field (2,5-heptadiene). (D) Snapshots of the SDPC (left) and DAPC (right) bilayer with chain double bonds shown in green.

(Figure 1C) was used to model two neighboring double bonds in SDPC and DAPC. The coupling between these neighboring dihedrals was strong; therefore, two-dimensional (2D) QM potential maps were calculated along ϕ_1 (C2═C3−C4−C5) and ϕ_2 (C3−C5−C5═C6) (Figure 1C). Details regarding the QM 2D maps and scheme used to obtain dihedral potentials are given in section 3.1. The Gaussian 03 suite of programs[21] was used in all these calculations with tight convergence in geometry optimizations (maximum force of 4.5×10^{-4}, and rms force of 3.0×10^{-4} hartree/bohr) and tight convergence in the single-point energies.

Molecular dynamics (MD) simulations of SDPC and DAPC bilayers were performed with starting conformations obtained from CHARMM-GUI *Membrane Builder*.[22,23] The size of the bilayer simulations with the C36 FF[20] and the revised FF, referred to as C36p, are shown in Table 1. The TIP3P water model consistent with the CHARMM FF[24,25] was used in all simulations. The van der Waals (vdW) interactions were smoothly switched off between 8 and 12 Å by a forced-based switching function. Long-range electrostatic interactions were calculated using the particle-mesh Ewald (PME) method.[26] An interpolation order of 4 and a direct space tolerance of 10^{-6} were used for the PME method. Equilibration of the CHARMM-GUI bilayers used the standard six-step equilibration process[23,27] of gradually turning off restraints on the lipids over 200 ps and were run with the CHARMM simulation program.[28]

All production runs were simulated until at least 25 ns of equilibrated trajectory data were obtained as indicated by the surface area per lipid. A tetragonal unit cell was used to maintain an equal dimension in X and Y (in the plane of the membrane), while Z varied independently in the NPT ensemble. A time-step of 2 fs was used with the SHAKE algorithm. The C36-based simulations were run in CHARMM, while the C36p simulations in NAMD.[29] For the CHARMM bilayer simulations, the temperature was held constant with the Hoover thermostat[30] and the pressure was maintained at 1 bar with the Nosé−Hoover piston.[31,32] For the NAMD bilayer simulations, Langevin dynamics was used to maintain constant temperatures for each system, while the Nosé−Hoover Langevin-piston algorithm[33,34] was used to maintain constant pressure at 1 bar. The Visual Molecular Dynamics (VMD)[35] program was used to create snapshots of the bilayers.

The bilayer simulations were analyzed for the surface area per lipid (SA), deuterium order parameters (S_{CD}), atomic form factors, electron density profiles (EDP), area compressibility modulus (K_A), and carbon−hydrogen relaxation times. The relative order of the hydrocarbon tails can be obtained from S_{CD}

$$|S_{CD}| = \left| \left\langle \frac{3}{2} \cos^2 \theta - \frac{1}{2} \right\rangle \right| \quad (1)$$

where θ is the angle of a C−H vector with respect to the bilayer normal. S_{CD} are typically reported as absolute values, and this is assumed in our abbreviation. The EDP was calculated using a binned method along the bilayer normal,[36] assuming minimal lipid membrane undulation for these relatively small bilayer patches. The atomic form factors compared directly with X-ray diffraction were calculated from these EDPs using the method previously described.[18] The K_A, a measure of the stiffness of the membrane, can be obtained from the SA together with their fluctuations via the following equation:[37]

dx.doi.org/10.1021/jp304056p | J. Phys. Chem. B 2012, 116, 9424−9431

Table 1. Detailed Information on the MD Simulations[a]

	SDPC (C36)	DAPC (C36)	SDPC (C36p)	DAPC (C36p)
# of atoms	30 914	33 057	17 157	17 538
# of lipids	128	128	72	72
# of waters	4246	5131	2311	2534
T [K]	303.15	303.15	297.15/303.15	303.15/323.15
Simulation time [ns]	50	50	50/50	50/100

[a]The simulation time is subdivided by the temperature.

$$K_A = k_B\langle T\cdot A\rangle/\sigma_A^2 \quad (2)$$

where k_B is the Boltzmann constant, T is the temperature, A is the system area, and σ_A^2 is the variance of the area during the simulation. ^{13}C spin−lattice relaxation ($1/T_1$) rates were calculated to compare with available experiments on SDPC and DAPC bilayers. The method used to find these rates is similar to other MD studies.[38−40] Assuming pure dipolar relaxation between the ^{13}C nucleus and its attached protons,[41]

$$\frac{1}{NT_1} = \frac{1}{10}\left(\frac{\hbar\gamma_c\gamma_h}{r_{C-H}^3}\right)^2[J(\omega_H - \omega_C) + 3J(\omega_C) + 6J(\omega_H + \omega_C)] \quad (3)$$

where N is the number of attached protons, r_{C-H} is the effective C−H bond length, γ_H and γ_C are the gyromagnetic ratios, and ω_H and ω_C are the Larmor frequencies. $J(\omega)$ is the spectral density given by

$$J(\omega) = \int_0^\infty C_2(t)\cos(\omega t)\,dt \quad (4)$$

$$C_2(t) = \langle P_2(\hat{\mu}(0)\cdot\hat{\mu}(t))\rangle \quad (5)$$

where $C_2(t)$ is the second rank reorientational correlation function, P_2 is the second-order Legendre polynomial, and $\hat{\mu}(t)$ is the unit vector along the C−H bond direction at time t. The integral in eq 4 was numerically found without fitting to a series of exponential functions.[39]

3. RESULTS AND DISCUSSION

3.1. Polyunsaturated Chain Force Field Development.

The recent C36 FF consisted of modifications to the saturated[42] and monounsaturated chains[20] and various dihedrals and charges in the headgroup region. However, the bilayer simulations of SDPC (containing polyunsaturated chain; Figure 1A) with the C36 FF in the NPT ensemble resulted in increased chain order and decreased SA compared to NMR and X-ray scattering data (see section 3.2 for details). Since SDPC only differs from previous C36-tested lipids with its PUFA chains, it seemed reasonable to determine whether changes to the torsions of neighboring double bonds were required. Some of the previous modifications to the CHARMM lipid FF[20,43,44] were based on high-level QM calculations[45] to scan important dihedrals. These QM dihedral energy profiles were either directly used to fit the dihedral potential in the CHARMM energy function, or used to guide choices in dihedral parameters to better match with experiment (such as previously done to match S_{CD} for DPPC bilayers in the C36 FF development).[20] Therefore, an identical approach was used to improve the dihedral potential for the neighboring double bonds in the PUFA chain.

Since QM calculations are extremely demanding, small model compounds are generally used to represent sections of the lipid to obtain accurate conformational energies with electron correlation. 2,5-Heptadiene (Figure 1C) was used to model the PUFA chain with emphasis on the two neighboring dihedrals ϕ_1 (C2═C3−C4−C5) and ϕ_2 (C3−C4−C5═C6). The model compound and dihedral angles were identical to the original parametrization for the PUFA chains in CHARMM.[8] However, the previous dihedral potentials were based on lower-level QM than in this study and limited dihedral scans, i.e., one-dimensional (1D) scans with one fixed dihedral. The hybrid methods for interaction energies (HM-IE)[45] approach was used to effectively result in QM energies at the CCSD(T)/cc-pVQZ level, compared to MP2/6-31 g(d,p) previously used.[8] The 2D scans on ϕ_1 and ϕ_2 were at 15° increments that resulted in a total of 576 QM energies (Figure 2, top). Two sample 1D scans are also shown in the Supporting Information (Figure S1).

The QM dihedral map shows minima at (ϕ_1, ϕ_2) of approximately (−120, +120)/(+120, −120), and equivalent minima, due to symmetry, at (+120, −120)/(−120, +120). These are fairly broad wells with a small barrier of 1−1.25 kcal/mol for transition between opposing wells. If the C36 FF was used for 2,5-heptadiene, the minima would be more constrained (Figure 2, middle). Although the placement of the two minima and preference to (+120, −120) was reproduced with C36, the breadth and transition barriers between the minima (∼3 kcal/mol) were in disagreement with the high-level QM calculations. Previous parametrization on alkanes in CHARMM[42,46] required increasing the well breadth while decreasing the transition barriers based solely on QM calculations. Therefore, we initially fit the dihedral potential (in CHARMM atom type format: CEL1-CEL1-CTL2-CTL2) to the CHARMM dihedral potential, $V\varphi$,

$$V_\varphi = \sum_j (K_{\varphi,j}(1 + \cos(n_j\varphi - \delta_j))) \quad (6)$$

where each dihedral, φ, can have j terms with $K_{\varphi,j}$ in kcal/mol, n_j is the periodicity, and δ_j is the phase shift. Fits directly to the QM calculations (C36q) were satisfactory, but MD simulations with SDPC bilayers resulted in too much chain order (Figure S2), especially for the *sn*-2 chain and smaller SA (68.7 ± 0.1 Å^2/lipid). Accuracies in the QM methods and assumptions of using a small model molecule are likely within 0.5−0.8 kcal/mol. Since the two wells have very low transitional barriers that can easily be sampled at temperatures of interest (290−310 K), adjusting the QM-based potential within these limits is reasonable if justified by experimental observables. Therefore, the transition barrier and breadth of the two minima (ϕ_1, ϕ_2) were changed to improve the agreement of chain order in comparison with NMR experiments, as explained in detail in the following section. The 2D dihedral map that best matches with the experiments, referred to as C36p, is shown in Figure 2 (bottom), and the parameters are shown in Table S1. The minima are broader than those estimated from CCSD(T)/cc-pVQZ, and the transition energy between the two minima is

dx.doi.org/10.1021/jp304056p | J. Phys. Chem. B 2012, 116, 9424−9431

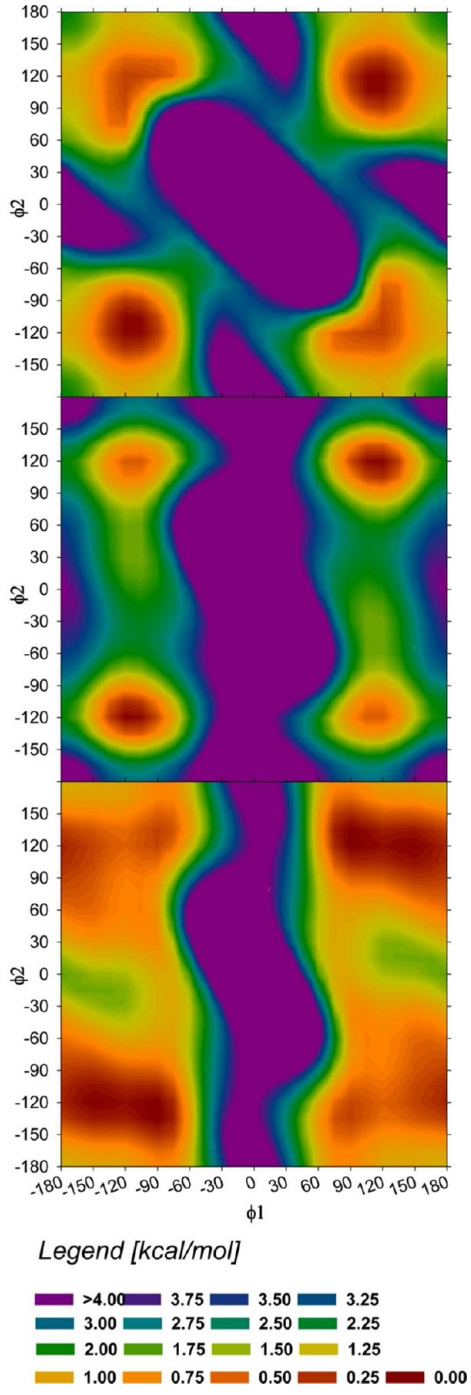

Figure 2. 2D maps of scans along ϕ_1 (C2═C3−C4−C5) and ϕ_2 (C3−C5−C5═C6) for 2,5-heptadiene: (top) CCSD(T)/cc-pVQZ, (middle) C36, and (bottom) C36p.

reduced to 0.5−0.8 kcal/mol. While the change may appear to be large between the QM and the C36p, at least for the two minima and the transition along a constant ϕ_2, this change is within the accuracy of our QM calculations (Figure S1). As shown in the following section, C36p agrees favorably for the S_{CD} in which we based our adjustment of the dihedral potential as well as various other structural lipid properties including the relaxation times for the PUFA chains.

3.2. MD Simulations of Lipid Bilayers. The increase in the well breadth for the minima in the dihedral potential surface (Figure 2) for C36p results in a better agreement with the experimental *sn*-1 and *sn*-2 S_{CD} of SDPC bilayers (Figure 3).[9] The saturated chain had significantly more order with the original C36 FF compared to our modification (C36p). This is also the case for the polyunsaturated chain (Figure 3, right), for which nearly complete disorder is better matched with C36p. While the C36p parameters were optimized to best represent the S_{CD} profiles of SDPC bilayers, it should be noted that the expected good agreement was achieved with a minimal change to the dihedral potential surface (i.e., less than 1 kcal/mol difference from QM calculations).

The S_{CD} are sensitive and anticorrelated to the SA,[36] i.e., the area would likely be lower for C36 than C36p based on the S_{CD} in Figure 3. A time series of these SA is shown in Figure S3 to demonstrate quick equilibration with bilayers of PUFA-containing lipids. A more specific example is shown in Table 2, where the average SA is 6.5 Å^2 lower for C36 compared to C36p at 303 K. X-ray scattering was previously used to obtain an estimate of the SDPC SA at 297 K (68.2 ± 0.4 Å^2/lipid),[9] which is in good agreement with our SDPC bilayer simulation at 297 K (69.7 ± 0.1 Å^2/lipid) in the NPT ensemble. Therefore, more precise and consistent SA was obtained using C36p compared to C36.

Form factors from C36 and C36p are compared to X-ray scattering of SDPC bilayers at 297 K in Figure 4. The agreement between experiment and simulation is best with the C36p FF (average root-mean square error (RMSE) of 0.18), while significant errors are associated with C36 FF (RMSE = 0.35). Direct comparison with experiment is achieved by the form factors, and additional insight is gained from the density profile that clearly shows the changes in the density as a function of depth in the membrane (Figure 5). For instance, the density at the center of the bilayer is slightly greater for C36p than for C36. The more noticeable difference is the head-to-headgroup spacing (D_{HH}) that is 39.3 ± 0.4 Å (C36p) and 41.7 ± 0.5 Å (C36) at 303 K. Furthermore, the D_{HH} for C36p at 297 K (38.6 ± 0.5 Å) is in excellent agreement with the experimental value (37.9 ± 0.1 Å).[9]

Since MD simulations with C36p were successful in reproducing various bilayer structural properties, we further analyzed our simulations to determine how our FF modifications influenced dynamical properties, i.e., NMR ^{13}C spin−lattice relaxation rate (T_1). For clarity, only C36p is shown in Figure 6. The agreement between experiment[9] and our MD simulations is excellent for all but the last few carbons in the PUFA chain, i.e., SDPC bilayer simulations with C36p have a higher spin−lattice relaxation time than experimental values for the end of the chain. These points have the least accuracy due to the quick decay of the $C_2(t)$ correlation function (in eq 5) and our rate of printing out coordinates (every 2 ps). Despite this, the trend of increasing T_1 as the acyl chain carbon number increases is well reproduced and, more importantly, the relaxation rates about the multiple unsaturated bounds are in good agreement with experiment. Therefore, our empirical adjustment of the dihedral potential appears to yield reasonable transitional barriers, which would result in incorrect NMR T_1 otherwise.

Simulations on DAPC bilayers were used to further validate our FF modifications on a lipid that contains two polyunsaturated chains, and compare properties between various lipid membranes. From MD simulations with C36p, replacing the saturated chain (in SDPC) with a polyunsaturated chain (in DAPC) results in a nearly 6 Å^2 increase in the SA (Table 2) at 303 K. On the other hand, MD simulations of

dx.doi.org/10.1021/jp304056p | J. Phys. Chem. B 2012, 116, 9424−9431

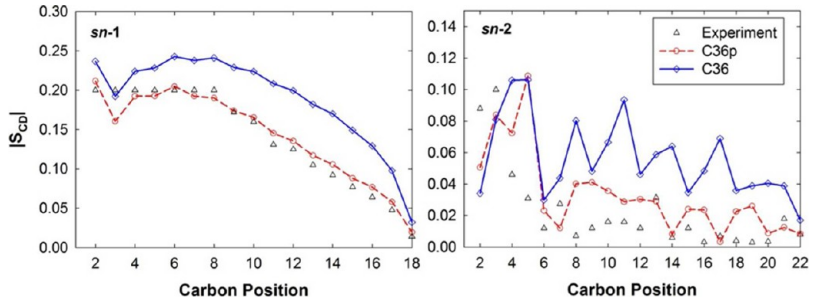

Figure 3. Deuterium order parameters (S_{CD}) from MD simulations for the *sn*-1 (saturated) and *sn*-2 (unsaturated) chains of SDPC at 303 K compared to experiment.[9]

Table 2. Average Surface Area Per Lipid (SA), Bulk Area Compressibility Modulus (K_A), and Head-to-Head Group Spacing (D_{HH}) with ± Standard Error[a]

lipid			SA [Å^2/lipid]	D_{HH} [Å]	K_A [dyn/cm]
SDPC	C36	303	63.2 ± 0.2	41.7 ± 0.5	163.9 ± 8.5
SDPC	C36p	297	69.7 ± 0.1	38.6 ± 0.5	285.7 ± 39.7
SDPC	C36p	303	70.8 ± 0.2	39.3 ± 0.4	218.2 ± 10.1
DAPC	C36	303	72.0 ± 0.2	37.6 ± 0.4	255.4 ± 30.4
DAPC	C36p	303	76.7 ± 0.2	36.4 ± 0.3	240.6 ± 0.2
DAPC	C36p	323	78.2 ± 0.2	36.4 ± 0.3	239.5 ± 6.2

[a]Experimental SA and D_{HH} of SDPC at 297 K are 68.2 ± 0.4 Å^2/lipid and 37.9 ± 0.1 Å, respectively.[9] The standard errors for SA were obtained based on 1 ns blocks and K_A based on 20 ns blocks with the first 10 ns not included in these averages and standard error estimates.

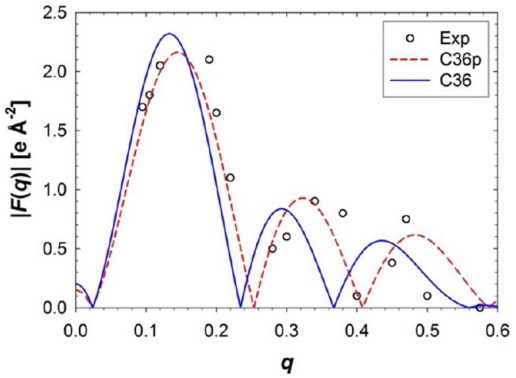

Figure 4. The calculated form factors, $F(q)$, compared to those obtained from X-ray at 297 K.[9] Note the MD simulations for C36p are at the experimental temperature, while C36 is at 303 K.

DAPC bilayers with C36 result in 4.7 Å^2 decrease in the SA (compared to C36p), indicating the higher chain order in C36 than in C36p even for DAPC. Although the C36p DAPC SA increases from 303 to 323 K by 1.5 Å^2 (Table 2), the thickness of the bilayer remains unaffected by this change. Moreover, the S_{CD} of DAPC at these two temperatures are equivalent until the end of the chain (after carbon-14), where there is an increase in chain disorder (decrease in S_{CD}) for both of the lipid chains (Figure S4). There is only limited experimental values to compare with for DAPC, i.e., NMR data at 323 K.[47] The calculated C36p spin−lattice relaxation times (Figure 6 (middle/bottom)) are in excellent agreement with the experimental values, and no discrepancy is shown for the end of the chains compared to SDPC. Discrepancies between experimental and simulated data decreased as the frequency of NMR experiments increased. As also shown in Figure 6, the

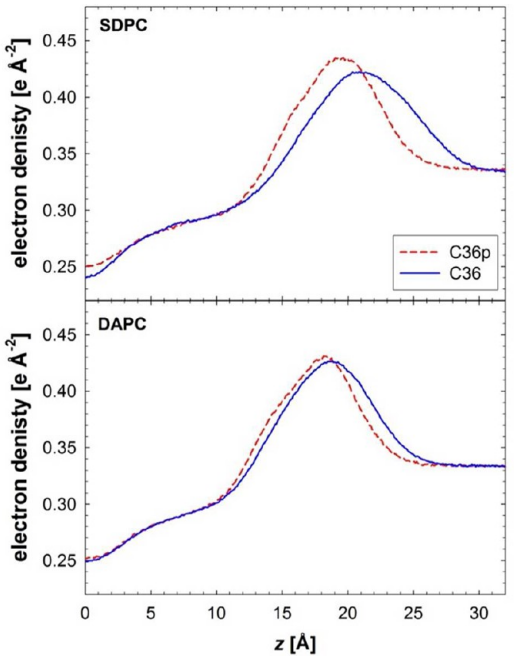

Figure 5. The calculated EDPs (symmetrized about the center of the bilayer) for SDPC (top) and DAPC (bottom) at 303 K.

relaxation dynamics is qualitatively similar for the PUFA chain in SDPC and DAPC, i.e., an increase in T_1 as the acyl chain carbon number increases.

The density profile difference between MD simulations with C36 and C36p is not as strong with DAPC compared to SDPC (Figure 5). The density at the center of the bilayer is nearly identical, and there is only a slight change in the D_{HH} (Table 2). The D_{HH} for a DAPC/cholesterol (90/10 mol %) bilayer (30.6 Å)[6] is significantly smaller than the values calculated from our C36p simulations without cholesterol (Table 2). Therefore, it appears that adding cholesterol has an expanding effect in terms of SA and decreases the headgroup peak spacing. Although the regions within the lipid bilayer have an overall similar distribution between SDPC and DAPC at 303 K, the component density of the unsaturated carbons in SDPC deviates from a Gaussian distribution with a higher probability at the bilayer center (Figure S5). However, when both chains are identical in unsaturation degree (DAPC), the density distribution for methylene reverts to a more Gaussian distribution. This may be important for structural model development in converting form factors to real-space densities with X-ray and neutron scattering,[48,49] because component distributions are assumed to be well approximated as a

dx.doi.org/10.1021/jp304056p | J. Phys. Chem. B 2012, 116, 9424−9431

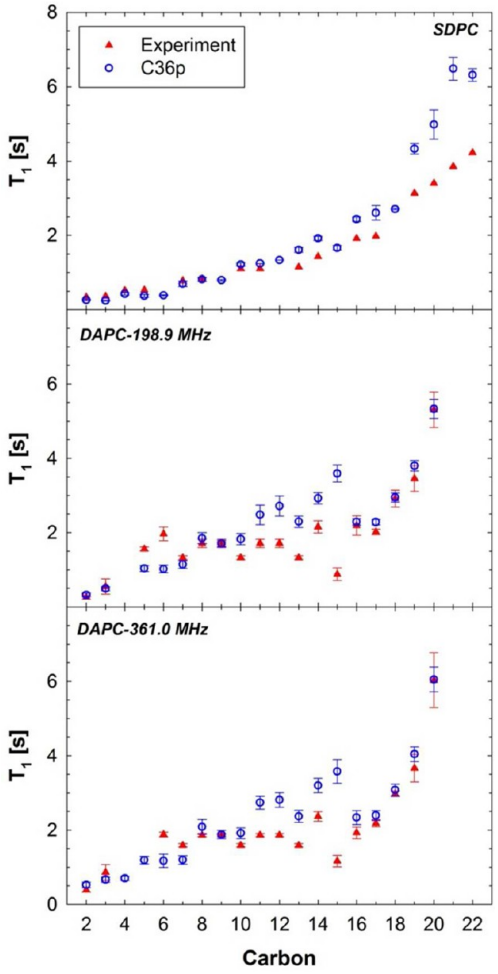

Figure 6. A comparison of the calculated (C36p) ^{13}C NMR T_1 for SDPC and DAPC with those from experiment (SDPC[9] and DAPC).

Gaussian in conventional models and this may not be the case with the unsaturated carbons of SDPC.

The level of unsaturation in a lipid's chain influences the density profile of the end methyl (Figure 7). A fully saturated lipid (DPPC) has a sharp peak at the center of the bilayer, but increasing the amount of unsaturation results in a decrease in this density. Consequently, the distribution becomes boarder

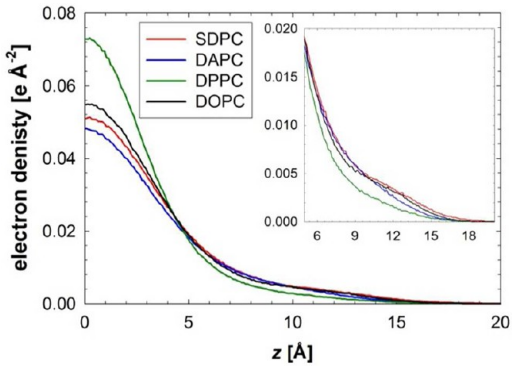

Figure 7. The electron density of the end methyl group in lipid bilayers (symmetrized about the center of the bilayer). Values for DPPC (323 K) and DOPC (303 K) were taken from previous MD simulations.[20]

with an increase kurtosis (non-Gaussian behavior) with elevated methyl density farther from the bilayer center. Although this is not surprising due to the flexible PUFA chains,[8] our simulations show that the probability of finding methyls far away from the bilayer center is similar between lipids with monounsaturated chains, such as DOPC, and lipids with polyunsaturated chains.

As a final comparative/test measurement, the bulk area compressibility modulus (K_A) was calculated for all of our MD simulations. The K_A of SDPC from C36 is lower than simulations with C36p, but statistically identical for DAPC (Table 2). The K_A for SDPC and DAPC are similar in a range of 220 to 280 dyn/cm and are also similar to DPPC simulations with C36 (236 ± 31 dyn/cm).[20] Although our MD simulations show minimal difference between DPPC and SDPC or DAPC, experimental estimates in the K_A for DAPC with micropipet techniques suggest values of 57 ± 17 dyn/cm at 288 K[50] and 106 ± 23 dyn/cm at 287 K.[51] This simulation/experimental disagreement is discussed in detail in the next section.

4. CONCLUSIONS

Previous parametrization of PUFA-containing lipids[8] was based on the C27 FF,[52,53] where the system size in *XY* was typically fixed during the simulations (the NPAT ensemble) due to deficiencies in modeling the lipid headgroup.[18,20] Several low-level QM 1D scans were used to fit PUFA dihedral potentials in C27 FF. These resulted in decent agreement with S_{CD}, but the order was higher than experiment. Moreover, these simulations required an *a priori* knowledge of the SA (assumed area of 65 Å^2/lipid for SDPC). MD simulations using the C27-based PUFA dihedral potentials but other parameters based on C36 resulted in similar issues, and NPT simulations resulted in elevated chain order and smaller SA when compared to experiment.

Therefore, an extension of the C36 FF[20] for lipids with polyunsaturated chains (C36p) was based on high-level QM calculations on the dihedral potential of 2,5-heptadiene (Figure 2) to improve chain order in PUFA-containing lipids. These QM dihedral maps indicated that the C27-based dihedral functions resulted in a too narrow distribution near the minima (Figure 2). Since chain S_{CD} were found to be sensitive to small changes (less than a kcal/mol) in this relatively flat energy surface near the four minima (Figure 2), empirical adjustments to the dihedral potential were made to improve agreement between SDPC S_{CD}. Consequently, there is an increase in chain disorder nearly identical to that observed for the *sn*-1 chain and similar for the highly disordered *sn*-2 chain (Figure 3). Similar improvement is observed in the results for DAPC disordered chains (Figure S4). There is excellent agreement between experiment and C36p for SDPC X-ray form factors and ^{13}C NMR relaxation times for both SDPC and DAPC bilayers.

The ^{13}C NMR relaxation times for SDPC with the C27-based simulations were overall similar to our new simulations with C36p. The T_1 were slightly overestimated for the end of the chain for C27, but underestimated for the chain carbons near the headgroup. The improvement of C36 compared to C27 was in the headgroup region; thus, it is expected that the C36p calculated T_1 would better match experiment in this region.

The calculated bulk K_A for phosphatidylcholine lipids with saturated and unsaturated chains was nearly identical to 200–280 dyn/cm (Table 2). Increasing chain unsaturation appears to have a negligible influence in the K_A. This is somewhat in

dx.doi.org/10.1021/jp304056p | J. Phys. Chem. B 2012, 116, 9424–9431

disagreement with experimental measurements at a lower temperature for DAPC vesicles (60−100 dyn/cm).[50,51] Since decreasing the temperature would likely result in an increase in K_A, temperature is likely not the cause for this disagreement. Our estimates in K_A are based on fluctuations in the simulation system area (σ_A^2 in eq 2) and require 20 ns blocks for convergence. Longer simulations or an alternative method based on a constant area isotherm[54] may reduce errors associated in these calculations. Another possible source of the error in our calculations is the small bilayer patch that may constrain some natural undulations in the bilayer and result in a too rigid membrane. Experimentally, PUFA-containing lipids can be oxidized and result in a less rigid membrane. Moreover, the large variation even in experimental K_A between laboratories[50,51] indicates difficulties in obtaining consistent values with the experimental technique. Although there are some conflicting results on the influence of chain unsaturation on elastic properties, we have shown that other changes in the acyl chain, based on the current parametrization scheme, result in an increased K_A. For example, chain branching and replacing a double bond with a cyclopropane moiety (lipids common in *Escherichia coli* cytoplasmic membranes) do result in more rigid membranes.[43,55] It appears roughness in these chains through branching can increase K_A and may have more of an influence compared to chain unsaturation.

Part of the motivation to improve the CHARMM PUFA FF was the lack in agreement between recent experiments on how cholesterol partitions in DAPC bilayers, i.e., stable formation of cholesterol parallel to the membrane surface at the bilayer center.[6,7] We (unpublished data) and others[12] have attempted with all-atom models to validate whether such thermodynamically stable orientations are indeed reproduced in MD simulations, but have not been successful. Moreover, we have previously shown that the free energy profile of cholesterol from its upright orientation to one being parallel to the membrane surface at the center bilayer does not pass though a minimum at the bilayer center.[56] Instead a transition state exists with cholesterol parallel to the membrane surface at the bilayer center. The free energy difference from cholesterol's upright to parallel position was calculated to be 5.4 kcal/mol. Since MD simulations of C36p with SDPC and DAPC result in an increase in chain disorder, this may enhance the stability of cholesterol in more parallel orientations. However, based on neutron scattering of DAPC+cholesterol bilayers,[6] a 6 Å decrease in head-to-head group spacing compared to our C36p pure DAPC bilayer simulation is required, suggesting a complex interaction between DAPC and cholesterol. C36p and recent modifications to the cholesterol force field in CHARMM[44] will allow us to further probe this unusual orientation of cholesterol in lipids with PUFA chains at the atomistic level.

■ ASSOCIATED CONTENT

Supporting Information

The SI contains figures of 1D scans for 2,5-heptadiene, SDPC S_{CD} with an intermediate QM-based force field, time series of lipid surface area, DAPC S_{CD}, component EDPs, and a table with updated CHARMM force field parameters. This information is available free of charge via the Internet at http://pubs.acs.org .

■ AUTHOR INFORMATION

Corresponding Author

*E-mail: jbklauda@umd.edu.

Notes

The authors declare no competing financial interest.

■ ACKNOWLEDGMENTS

This work was supported in part by institutional funding from the University of Maryland (J.B.K.) and NSF MCB-0918374 (W.I.). This research was also supported in part by the National Science Foundation through TeraGrid/XSEDE resources provided by the National Institute for Computational Sciences under Grant Number TG-MCB100139 (J.B.K.) and TG-MCB110072 (W.I.). Additional computational resources were used on the High Performance Computing Cluster at the University of Maryland (J.B.K.). Quantum calculations utilized the high-performance computational capabilities of the Biowulf Linux cluster at the National Institutes of Health, Bethesda, MD (http://biowulf.nih.gov). The authors would like to thank Nadukkudy Eldho for proving the experimental values for S_{CD} on SDPC bilayers.

■ REFERENCES

(1) Engelman, D. M. *Nature* **2005**, *438*, 578.
(2) McMahon, H. T.; Gallop, J. L. *Nature* **2005**, *438*, 590.
(3) Jordan, J. D.; Landau, E. M.; Iyengar, R. *Cell* **2000**, *103*, 193.
(4) Hunter, T. *Cell* **2000**, *100*, 113.
(5) Pollock, S.; Nichita, N. B.; Bohmer, A.; Radulescu, C.; Dwek, R. A.; Zitzmann, N. *Proc. Natl. Acad. Sci. U.S.A.* **2010**, *107*, 17176.
(6) Harroun, T. A.; Katsaras, J.; Wassall, S. R. *Biochemistry* **2006**, *45*, 1227.
(7) Harroun, T. A.; Katsaras, J.; Wassall, S. R. *Biochemistry* **2008**, *47*, 7090.
(8) Feller, S. E.; Gawrisch, K.; MacKerell, A. D. *J. Am. Chem. Soc.* **2002**, *124*, 318.
(9) Eldho, N. V.; Feller, S. E.; Tristram-Nagle, S.; Polozov, I. V.; Gawrisch, K. *J. Am. Chem. Soc.* **2003**, *125*, 6409.
(10) Feller, S. E.; Gawrisch, K.; Woolf, T. B. *J. Am. Chem. Soc.* **2003**, *125*, 4434.
(11) Pitman, M. C.; Suits, F.; MacKerell, A. D.; Feller, S. E. *Biochemistry* **2004**, *43*, 15318.
(12) Marrink, S. J.; deVries, A. H.; Harroun, T. A.; Katsaras, J.; Wassall, S. R. *J. Am. Chem. Soc.* **2008**, *130*, 10.
(13) Kucerka, N.; Marquardt, D.; Harroun, T. A.; Nieh, M.-P.; Wassall, S. R.; de Jong, D. H.; Schafer, L. V.; Marrink, S. J.; Katsaras, J. *Biochemistry* **2010**, *49*, 7485.
(14) Carrillo-Tripp, M.; Feller, S. E. *Biochemistry* **2005**, *44*, 10164.
(15) Pitman, M. C.; Grossfield, A.; Suits, F.; Feller, S. E. *J. Am. Chem. Soc.* **2005**, *127*, 4576.
(16) Grossfield, A.; Feller, S. E.; Pitman, M. C. *J. Phys. Chem. B* **2006**, *110*, 8907.
(17) Grossfield, A.; Feller, S. E.; Pitman, M. C. *Proc. Natl. Acad. Sci. U. S. A.* **2006**, *103*, 4888.
(18) Klauda, J. B.; Kučerka, N.; Brooks, B. R.; Pastor, R. W.; Nagle, J. F. *Biophys. J.* **2006**, *90*, 2796.
(19) Benz, R. W.; Castro-Roman, F.; Tobias, D. J.; White, S. H. *Biophys. J.* **2005**, *88*, 805.
(20) Klauda, J. B.; Venable, R. M.; Freites, J. A.; O'Connor, J. W.; Mondragon-Ramirez, C.; Vorobyov, I.; Tobias, D. J.; MacKerell, A. D.; Pastor, R. W. *J. Phys. Chem. B* **2010**, *114*, 7830.
(21) Frisch, M. J.; Trucks, G. W.; Schlegel, H. B.; Scuseria, G. E.; Robb, M. A.; Cheeseman, J. R.; Montgomery, J. A., Jr.; Vreven, T.; Kudin, K. N.; Burant, J. C.; et al. *Gaussian 03*, revision B.03; Gaussian, Inc: Pittsburgh, PA, 2003.
(22) Jo, S.; Kim, T.; Iyer, V. G.; Im, W. *J. Comput. Chem.* **2008**, *29*, 1859.
(23) Jo, S.; Lim, J. B.; Klauda, J. B.; Im, W. *Biophys. J.* **2009**, *97*, 50.
(24) Durell, S. R.; Brooks, B. R.; Bennaim, A. *J. Phys. Chem.* **1994**, *98*, 2198.

(25) Jorgensen, W. L.; Chandrasekhar, J.; Madura, J. D.; Impey, R. W.; Klein, M. L. *J. Chem. Phys.* **1983**, *79*, 926.
(26) Darden, T.; York, D.; Pedersen, L. *J. Chem. Phys.* **1993**, *98*, 10089.
(27) Jo, S.; Kim, T.; Im, W. *PLoS One* **2007**, *2*, e880.
(28) Brooks, B. R.; Brooks, C. L.; Mackerell, A. D.; Nilsson, L.; Petrella, R. J.; Roux, B.; Won, Y.; Archontis, G.; Bartels, C.; Boresch, S.; et al. *J. Comput. Chem.* **2009**, *30*, 1545.
(29) Phillips, J. C.; Braun, R.; Wang, W.; Gumbart, J.; Tajkhorshid, E.; Villa, E.; Chipot, C.; Skeel, R. D.; Kale, L.; Schulten, K. *J. Comput. Chem.* **2005**, *26*, 1781.
(30) Hoover, W. G. *Phys. Rev. A* **1985**, *31*, 1695.
(31) Nosé, S.; Klein, M. L. *J. Chem. Phys.* **1983**, *78*, 6928.
(32) Andersen, H. C. *J. Chem. Phys.* **1980**, *72*, 2384.
(33) Feller, S. E.; Zhang, Y.; Pastor, R. W.; Brooks, B. R. *J. Chem. Phys.* **1995**, *103*, 4613.
(34) Martyna, G. J.; Tobias, D. J.; Klein, M. L. *J. Chem. Phys.* **1994**, *101*, 4177.
(35) Humphrey, W.; Dalke, A.; Schulten, K. *J. Mol. Graphics* **1996**, *14*, 33.
(36) Feller, S. E.; Venable, R. M.; Pastor, R. W. *Langmuir* **1997**, *13*, 6555.
(37) Feller, S. E.; Pastor, R. W. *J. Chem. Phys.* **1999**, *111*, 1281.
(38) Klauda, J. B.; Roberts, M. F.; Redfield, A. G.; Brooks, B. R.; Pastor, R. W. *Biophys. J.* **2008**, *94*, 3074.
(39) Klauda, J. B.; Eldho, N. V.; Gawrisch, K.; Brooks, B. R.; Pastor, R. W. *J. Phys. Chem. B* **2008**, *112*, 5924.
(40) Pastor, R. W.; Venable, R. M.; Feller, S. E. *Acc. Chem. Res.* **2002**, *35*, 438.
(41) Lipad, G.; Szabo, A. *J. Am. Chem. Soc.* **1982**, *104*, 4546.
(42) Klauda, J. B.; Brooks, B. R.; MacKerell, A. D., Jr.; Venable, R. M.; Pastor, R. W. *J. Phys. Chem. B* **2005**, *109*, 5300.
(43) Pandit, K. R.; Klauda, J. B. *Biochim. Biophys. Acta, Biomembr.* **2012**, *1818*, 1205.
(44) Lim, J. B.; Rogaski, B.; Klauda, J. B. *J. Phys. Chem. B* **2012**, *116*, 203.
(45) Klauda, J. B.; Garrison, S. L.; Jiang, J.; Arora, G.; Sandler, S. I. *J. Phys. Chem. A* **2004**, *108*, 107.
(46) Klauda, J. B.; Pastor, R. W.; Brooks, B. R. *J. Phys. Chem. B* **2005**, *109*, 15684.
(47) Zajíček, J.; Ellena, J. F.; Williams, G. D.; Khadim, M. A.; Brown, M. F. *Collect. Czech. Chem. Commun.* **1995**, *60*, 719.
(48) Klauda, J. B.; Brooks, B. R.; Pastor, R. W. *J. Chem. Phys.* **2006**, *125*, 144710.
(49) Kučerka, N.; Nagle, J. F.; Sachs, J. N.; Feller, S. E.; Pencer, J.; Jackson, A.; Katsaras, J. *Biophys. J.* **2008**, *95*, 2356.
(50) Needham, D.; Nunn, R. S. *Biophys. J.* **1990**, *58*, 997.
(51) McIntosh, T. J.; Advani, S.; Burton, R. E.; Zhelev, D. V.; Needham, D.; Simon, S. A. *Biochemistry* **1995**, *34*, 8520.
(52) Feller, S. E.; MacKerell, A. D., Jr. *J. Phys. Chem. B* **2000**, *104*, 7510.
(53) Feller, S. E.; Yin, D. X.; Pastor, R. W.; MacKerell, A. D., Jr. *Biophys. J.* **1997**, *73*, 2269.
(54) Venable, R. M.; Skibinsky, A.; Pastor, R. W. *Mol. Simul.* **2006**, *32*, 849.
(55) Lim, J. B.; Klauda, J. B. *Biochim. Biophys. Acta, Biomembr.* **2011**, *1808*, 323.
(56) Jo, S.; Rui, H.; Lim, J. B.; Klauda, J. B.; Im, W. *J. Phys. Chem. B* **2010**, *114*, 13342.